

Performance of Ni, Pt, and Pd Monometal and Ni-Pt Bimetal onto Activated Carbon for Hydrocracking of Castor Oil

Wega Trisunaryanti^a, Iip Izul Falah^a, Siti Khoirun Nasi'ah^a, Satriyo Dibyo Sumbogo^a

a) Department of Chemistry, Faculty of Mathematics and Natural Science, University Gadjah Mada, Yogyakarta, Indonesia

Received 30 July 2023; received in revised form 26 November 2023; accepted 28 December 2023 (DOI: 10.30495/IJC.2023.1992636.2032)

ABSTRACT

The development of high-performance hydrotreating catalysts has been a challenging pursuit within the catalyst research field. In this study, activated carbon was synthesized chemically, utilizing oxygen gas as the activator and Merbau wood as the precursor. Subsequently, the activated carbon was impregnated with both mono (Ni, Pt, Pd) and bimetallic (NiPt) species. Physical activation employing oxygen gas was employed in the preparation of the activated carbon. Notably, the optimum activation temperature using oxygen gas was identified at 350°C, aligning with the peak iodine value of 3989.7 mg/g. Subsequently, the activated carbon served as a highly efficient support material for the hydrocracking of castor oil. Among the investigated catalysts, the NiPt/AC catalyst emerged as the most promising, achieving a remarkable liquid fraction conversion of 88.73 wt%. However, it is crucial to acknowledge that the NiPt/AC catalyst exhibited limitations in terms of stability, experiencing sintering and performance degradation after only three usage cycles.

Keywords: *Biofuels, Activated carbon, Hydrocracking, Castor oil*

1. Introduction

The ever-increasing global demand for cleaner energy sources and sustainable feedstocks has steered the focus of hydrocracking research towards renewable alternatives. Currently, biodiesel fuel production is heavily relied on vegetable oils as their primary source. However, the current selection of vegetable oils still competes with food supplies, as they are predominantly cultivated on agricultural farming land [1-4]. The diversification and usage of non-edible eating oil could solve the resource problem; the choice could fall on jatropha, rubber seed, Callophyllom inophyllum, castor, etc [5-10]. Castor oil is one of the strongest candidates as its trees do not require a lot of watering, can grow on marginal soils, and has high oil content. Its significant composition of triglycerides, predominantly featuring ricinoleic acid 86-92%, distinguishes castor oil from conventional vegetable oils, rendering it a compelling candidate for catalytic conversion processes into biofuel. Castor oil itself comprises of 88.9% tricoinolein

acid, 4.5% trilinolein acid, 3.5% triolein acid, 1.4% tripalmitin acid, 0.9% tristearin acid, and 0.3% trillionolenin acid [9-13].

The conversion of the dominant ricinoleic acid into a viable biofuel can be achieved through cracking and/or dehydrogenation-deoxygenation processes [14-16]. Cracking facilitates the cleavage of the fatty acid into shorter fatty acids and low-chain hydrocarbons. This cracking reaction can be catalytic or hydrocracking in nature, with hydrocracking gaining more prominence due to its longer catalyst lifetime compared to catalytic cracking [14]. The hydrocracking catalysts employed are typically bifunctional, containing metals responsible for catalyzing the cracking reactions [17-20]. Some of these metals also exhibit hydrodeoxygenation and dehydrogenation capabilities, which are essential for transforming ricinoleic acid into valuable biofuel products. Commonly used catalysts for these reactions are noble metals such as Pt and Pd, or sulfided VI-VII elements [21-25]. However, these metal catalysts are susceptible to deactivation at elevated temperatures, as they tend to aggregate and form larger clusters, thereby

*Corresponding author:

E-mail address: wegats@ugm.ac.id (W. Trisunaryanti)

reducing the active surface area of the catalyst [26]. Consequently, it becomes imperative to prevent metal aggregation at high operating temperatures to maintain catalyst effectiveness.

Activated carbon emerges as a robust candidate for serving as a support material, primarily due to its ability to be derived from cost-effective sources and the ease with which its porosity properties can be fine-tuned [27-28]. The abundance of Merbau wood in Indonesia makes it a suitable choice for a lignocellulosic precursor in the production of activated carbon. [29]. In addition to the imperative role of acid sites during the hydrocracking process, the catalyst's overall catalytic performance is notably influenced by the efficient mass transport of feed molecules within the catalytic structure [30-32]. Given that the size of lipid molecules generally exceeds 2 nm, rendering them too large for effective micropore utilization, catalytic conversion cannot be fully optimized [33]. The optimization of activated carbon properties can be achieved through the activation process, commonly accomplished by employing either physical methods, such as the use of oxidizing gases like steam, CO₂, or air, or chemical treatments involving acids, bases, and alkaline metals [34-37]. The physical treatments offer the advantage of straightforward procedures without involving chemical reactions, thus eliminating the need for corrosive substances during the activation process, thereby ensuring ease of handling and a cleaner activation process [38-39].

No research has yet confirmed that activated carbon from O₂ activation is suitable to host monometallic nor bimetallic catalyst systems for hydrocracking applications of vegetable oils. This study encompassed a comprehensive investigation aimed at determining the optimal activating temperature using oxygen gas to maximize the surface area obtained from Merbau wood, employed as the lignocellulosic source. Additionally, the intricate interplay between mono and bimetallic catalysts of noble metal and Ni metal with microporous support was thoroughly examined to ascertain their potential as effective hydrotreatment catalysts for castor oil. Furthermore, special attention was devoted to assessing the catalyst's reusability, particularly considering the inherent coking potential associated with microporous supports.

2. Experimental

2.1 Materials and Chemicals

The waste woods used in this research was obtained from Manokwari, Papua barat. The castor oil used for hydrotreatment was obtained from a local store. AgNO₃,

Ni (NO₃)₂·6H₂O, PdCl₂, and PtCl₄ were supplied by Merck and used without further purification. The gases used in this research (i.e., H₂ and N₂) were supplied by PT Surya Indotim Imex.

2.2 Synthesis of Activated Carbon

The synthesis method of activated carbon in this study was conducted using Merbau wood sawdust waste. The sawdust from Merbau wood was subjected to a drying process in an oven at 105°C for a duration of 48 hours. Dried Merbau wood with a mass of 30 grams was carbonized in a furnace at 800 °C under a flow of N₂ gas at a rate of 20 mL/min for 2 hours, resulting in the formation of charcoal. The produced charcoal was then pulverized into powder and sieved using an 80-mesh sieve. The charcoal powder that passed through the 80-mesh sieve, amounting to 20 grams, was further subjected to activation using O₂ gas at flow rates of 15 mL/min at temperatures of 250, 350, and 450 °C successively for 2 hours each, yielding three samples of activated carbon (AC) labeled as AC-250, AC-350, and AC-450, respectively. Subsequently, each activated carbon sample was sieved, washed with acetone for 2 hours, and dried in an oven at 100 °C for 24 hours. The dried activated carbon samples were then immersed in a 1 M HCl solution for 2 hours, followed by washing with deionized water until no precipitate formed when the filtrate was treated with AgNO₃. The presence of white precipitate indicates the residual chloride left inside the activated carbon. Finally, all the activated carbon samples were dried in an oven at 100 °C for 24 hours.

2.3 Metal Impregnation onto AC

A total of 0.4459 g of Ni (NO₃)₂·6H₂O was accurately weighed and introduced into 100 mL deionized water containing 3.00 g of activated carbon (AC) via the wet impregnation method. The impregnation procedure involved mixing the metal salt and the support material for 24 hours, followed by solvent evaporation at 100°C until complete solvent removal was achieved. Subsequently, the resulting materials were subjected to a reduction reaction at 550°C under a flowing stream of H₂ gas at a rate of 20 cc/min. The synthesis of Pd/AC and Pt/AC followed a similar approach, employing 15.25 mg (0.3 wt%) and 15.54 mg (0.3 wt%) of the respective salt precursors, respectively. As for the bimetallic catalyst Ni-Pd/AC, it was synthesized by dispersing precisely 0.4459 g of Ni (NO₃)₂·6H₂O and 15.25 mg of PdCl₂ into a 100 mL deionized water containing 3.00 g of AC support material. This preparation method is referring to our previous study [8, 15, 20-22].

2.4 Catalyst Characterization

Characterization of functional groups present in the char and activated carbon (AC) was carried out using Fourier transform infrared spectroscopy (FTIR) on a Shimadzu Prestige 21 instrument. The morphological analysis of the char, AC, Ni/AC, Pt/AC, Pd/AC, and NiPt/AC samples was performed using scanning electron microscopy with energy-dispersive X-ray mapping (SEM-EDX) on a JEOL JSM-6510LA instrument. X-ray diffractometry (XRD) on an X'Pert PRO PANalytical system was employed to identify the amorphous phase of AC and the crystalline phases of the metal catalysts. To determine the porosity of the catalysts, surface area analysis was conducted using a QuadraSorb Station 2 surface area analyzer. Additionally, the acidity of the catalysts was determined gravimetrically through the adsorption of NH₃ vapor as a basic adsorbate, following equation (1).

$$\text{Acidity} = \frac{W_2 - W_1}{(W_1 - W_0)Mr} \times 1000 \frac{\text{mmol}}{\text{g}} \quad (1)$$

W₀ = Weight of empty container
 W₁ = Weight of dried catalyst and container
 W₂ = Weight of the catalyst and container after adsorption
 Mr = Molecular weight of pyridine

2.5 Hydrotreatment of Castor Oil

Catalyst performance evaluation was conducted using a semi-fixed batch reactor operating under a continuous flow of hydrogen gas. The hydrocracking reactor schematic are shown in **Fig. 1**. The catalyst was carefully positioned in a stainless-steel holder, placed above the feed, with a catalyst-to-feed ratio of 1:100. The hydrotreatment process was carried out for a duration of 2 hours at a temperature of 550°C, with a constant flow of hydrogen gas set at 20 mL/min. Subsequently, the products obtained from the hydrotreatment were subjected to comprehensive analysis utilizing gas chromatography-mass spectrometry (GC-MS) on a Shimadzu QP2010S instrument with 300°C as its operational temperature.

For the purpose of characterization, the hydrocarbon compounds in the obtained products were categorized into gasoline and diesel fractions, encompassing carbon numbers ranging from C₄ to C₁₂ and C₁₃ to C₂₀, respectively. Additionally, the alcohol fraction was defined to encompass alcohol compounds of any carbon number, while all other compounds, excluding hydrocarbons and alcohols, were categorized separately as others. The remaining feed was quantified by determining the residue. This meticulous assessment of

the catalytic performance and product analysis provides valuable insights into the effectiveness of the catalyst in converting the feedstock into desired hydrocarbon and alcohol fractions, thereby contributing to the understanding and advancement of the hydrotreatment process for potential application in the production of gasoline, diesel, and other valuable products.

$$\text{Residue} = \frac{W_R}{W_F} \times 100\% \quad (3)$$

$$\text{Liquid fraction (wt\%)} = \frac{W_P}{W_F} \times 100\% \quad (4)$$

$$\text{Coke} = \frac{W_{C_2} - W_{C_1}}{W_F} \times 100\% \quad (5)$$

$$\text{Gas} = 100\% - (\text{liquid fraction} + \text{coke} + \text{residue}) \quad (6)$$

$$\text{Gasoline} = (\% \text{ Area of } C_5 \text{ to } C_{12}) \times \text{liquid fraction} \quad (7)$$

$$\text{Diesel Oil} = (\% \text{ Area of } C_{13} \text{ to } C_{20}) \times \text{liquid fraction} \quad (8)$$

$$\text{Other fraction} = \text{Liquid fraction} - (\text{Gasoline} + \text{Diesel Oil}) \quad (9)$$

W_R = Weight of unconverted the feed

W_F = Weight of the feed

W_{C1} = Weight of the catalyst before hydrotreatment

W_{C2} = Weight of the catalyst after hydrotreatment

W_R is the weight of unconverted feed, W_F is the weight of the feed, W_{C1} is the weight of the catalyst before hydrotreatment, and W_{C2} is the weight of the catalyst after hydrotreatment.

3. Results and Discussion

3.1 Synthesis of Activated Carbon

Fig. 2 displays the iodine values of both char (C) and activated carbon (AC). The iodine value was employed as a means to assess and compare the surface areas of the resulting activated carbon samples, as the iodine adsorption value is directly correlated with surface area. Remarkably, the highest iodine value was attained through the activation of char material at a relatively low temperature of 350°C, utilizing O₂ gas as an activating agent. The introduction of O₂ gas during the activation process facilitated the oxidation and perforation of the carbon material, thereby leading to a significant increase in the surface area. Elevated activation temperatures have been observed to induce excessive perforation of the carbon material, leading to structural collapse and consequent reduction in its surface area. This mechanism of activation not only enhanced the surface area but also contributed to the development of acidic functional groups in the activated carbon. Further discussions regarding the FTIR and acidity data will

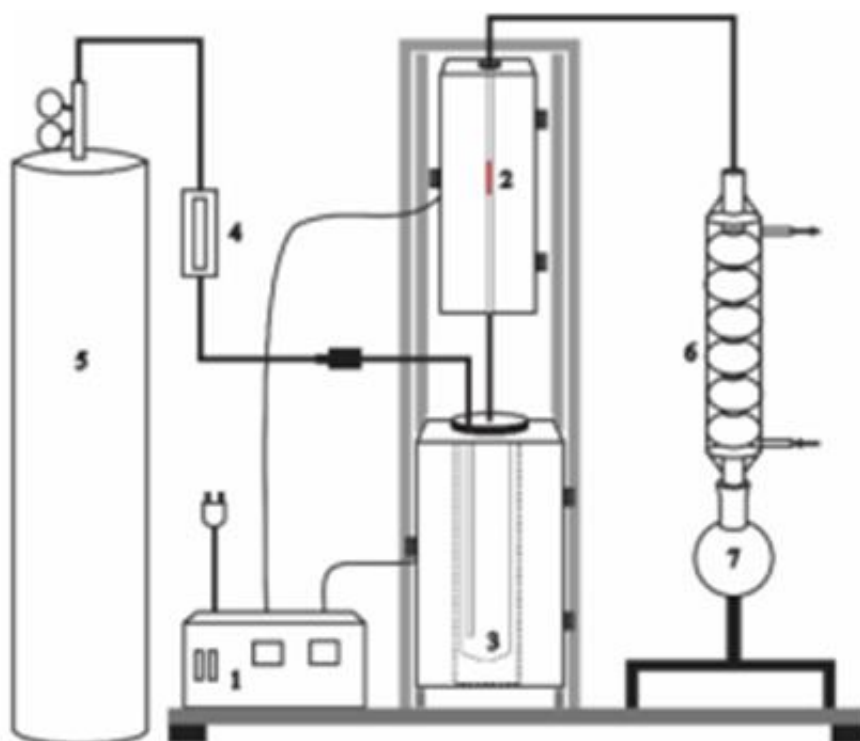


Fig. 1. Reactor design for hydrocracking application, 1: Heat controller, 2: Catalyst chamber, 3: Feedstock chamber, 4: Gas flowmeter, 5: Hydrogen gas tank, 6: Condensor, 7: Product collecting flask

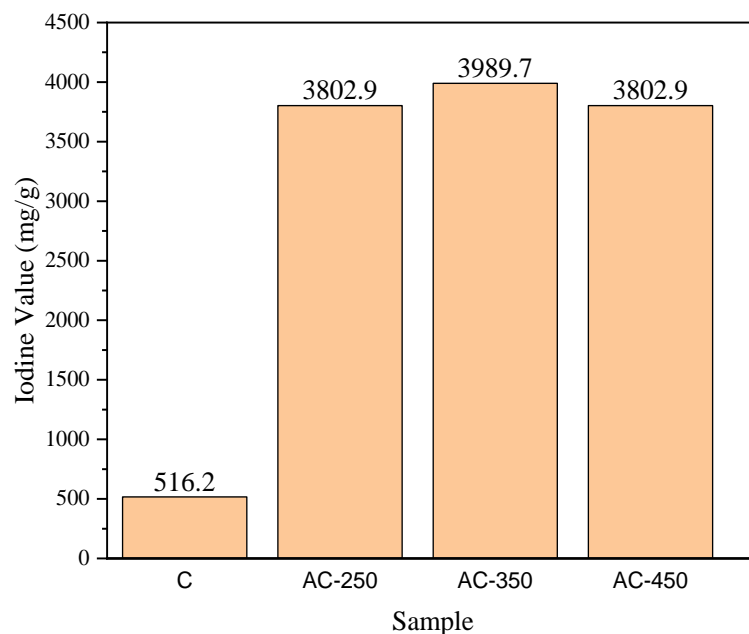


Fig. 2. The Iodine value of Char (C) and Activated Carbon (AC-250, AC-350, AC-450)

shed light on these observed functional groups and their implications in the overall catalytic behavior of the activated carbon.

Functional groups of C and AC are shown in **Fig. 3**. The charring process of lignocellulosic material facilitates the emergence of amide functional groups as the predominant moiety within the material. However, upon

activation of char using O₂ gas, excessive oxidation of the material occurs, leading to the conversion of amide groups into carbonyl groups, evident through the conspicuous absence of the amide II and III peaks at 1455 and 1385 cm⁻¹, respectively. Conversely, there were no significant differences in the hydroxyl group among the different materials, as indicated by the characteristic peak at 3455 cm⁻¹. These findings elucidate the intricate transformation of functional groups during the activation process and contribute to a comprehensive understanding of the chemical modifications occurring in char and activated carbon samples.

The diffractogram of the char sample exhibited a trace presence of crystalline material, likely originating from the lignocellulosic source. As this trace metal was deemed irrelevant to the hydrocracking performance, a leaching process was employed to eliminate the inorganic crystals before the activation step using O₂ gas. Subsequently, a subtle disparity in crystallinity was observed between the activated carbon (AC) and the char, with the amorphous peak of the AC slightly higher in intensity compared to the char. The considerable increase in the iodine adsorption value and the

discernible alterations in the functional groups strongly indicate the successful synthesis of activated carbon (AC), making it a viable candidate for application as a metal support material. As shown in **Table 1**, activation using O₂ gas did not increase the surface area significantly; compared to another previous journal, it was quite low. However, the presence of a high iodine value that was not accompanied by its high surface area becomes something interesting to discuss, as the functional group in the support material has the potential to become a catalyst due to the high amount of functional group. Typical activated carbon that has an iodine value of 500-1200 mg/g usually has a surface area of 900-1100 m²/g [40]. The observed misalignment may be explained by the carbon material undergoing significant oxidation without causing substantial perforation of its surface. It was also noted that the synthesized activated carbon from this research has extremely lower surface area and acidity compared to our previous study on activated carbon but higher iodine value [8, 15, 29]. These features give this carbon support material uniquely selective for the decarboxylation reaction of ricinoleic acid, which is discussed in the next sub-chapter.

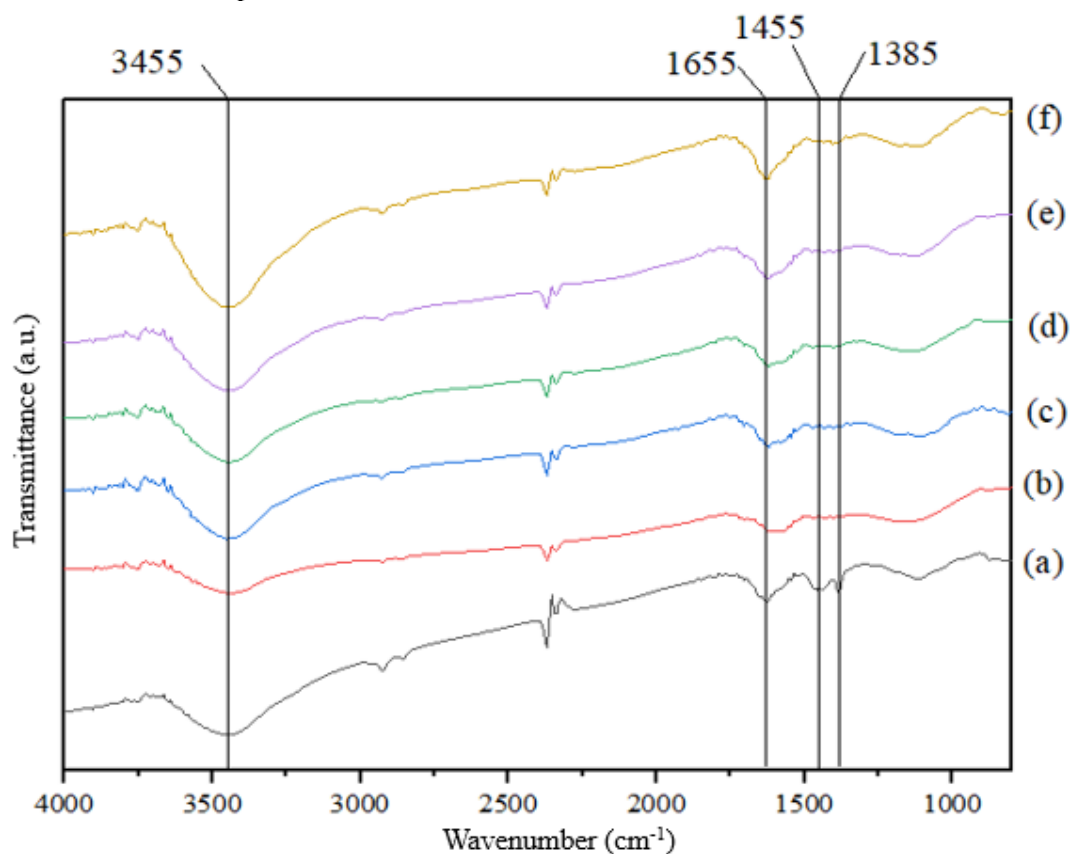


Fig. 3. FTIR spectra of (a) C, (b) AC, (c) Ni/AC, (d) NiPt/AC, (e) Pt/AC, (f) Pd/AC catalyst

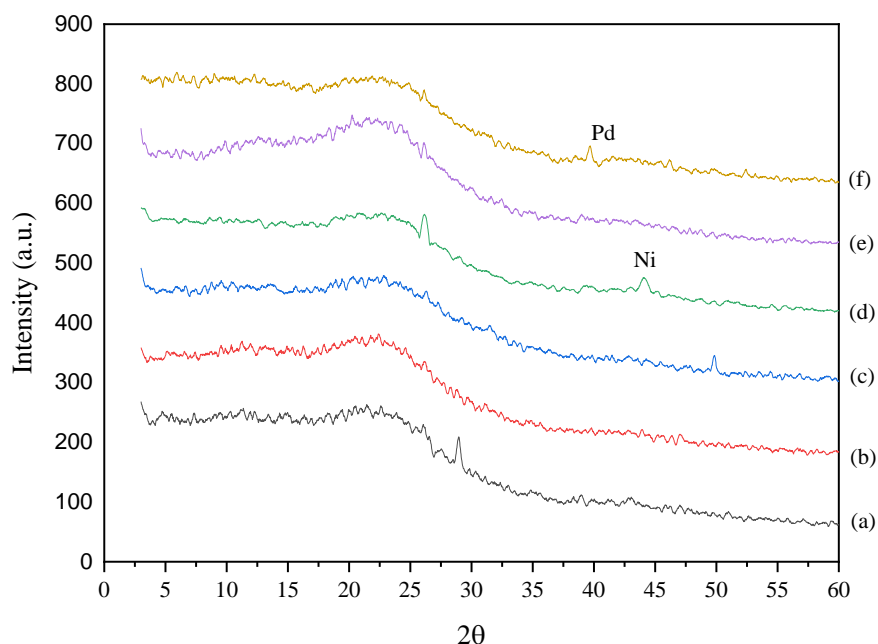


Fig. 4. Diffractogram of (a) C, (b) AC, (c) Ni/AC, (d) NiPt/AC, (e) Pt/AC, (f) Pd/AC catalyst

3.2 Metal Impregnation

The impregnated metal inside the catalyst gives its own unique diffractogram peak, as shown in **Fig. 4**. Based on the additional peaks that exist in the diffractogram, only Ni in NiPt/AC and Pd in Pd/AC that are present as reduced form. The additional peak of Ni metal at 2θ 44.28° , which attributed to Ni (ICDD No. 00-045-1027). The Pd metal additional peak showed at 2θ 40.02° that attributed to Pd (ICDD No. 01-087-0637). The complete absence of Pt metal additional peak could be caused by the small size of the non-crystalline impregnated Pt metal [15]. This non-crystalline form did not give diffraction as they do not have perfect lattices. This phenomenon could be contributed to the low concentration of Pt and/or the evenly distributed Pt across our activated carbon material.

An intriguing observation pertaining to the acidity data of the catalyst is evident from the findings in **Table 1**. Notably, the impregnation of mono-metal contributes to the enhancement of the catalyst's acidic characteristics, whereas bimetal impregnation leads to a reduction in the catalyst's acidity. Interestingly, this phenomenon is not attributed to pore-blocking effects, as evidenced by the increased surface area and pore volume observed in the NiPt/AC catalyst. When impregnating mono-metal catalysts, the metal may disperse more uniformly on the support material, leading to a higher concentration of active sites, which can enhance the acidity. On the other hand, in bimetal catalysts, the metals might interact

differently with the support, leading to varied dispersion and potentially fewer available active sites, resulting in reduced acidity.

The mesoporous characteristic of both the catalyst and its carbon matrix is observed through the hysteresis plot presented in **Fig. 5**. The porosity data of the catalyst investigated in this study have been meticulously documented in **Table 1**. Notably, intriguing phenomena have been observed in relation to the presence of Pt metal, both in its monometallic and bimetallic forms. The impregnation of Pt onto the AC support exhibited a noteworthy outcome, as it did not induce any discernible addition of diffractogram peaks. This observation suggests that the Pt metal dispersion was effectively homogeneous, signifying a favorable and well-distributed dispersion. Furthermore, this unique phenomenon contributed to additional textural modifications of the catalyst, consequently bestowing an augmented surface area to the catalytic material. The extra textural property that the Pt metal gives is also creating more microporous to the catalyst, as there is an increment in the micropore volume.

In terms of the porosity data, Pt/AC and NiPt/AC was the two of the best catalyst among the other, with the Pt/AC having more acidity compared to NiPt/AC. This difference in the chemical properties of a catalyst will ultimately affect the catalyst hydrocracking performance of castor oil.

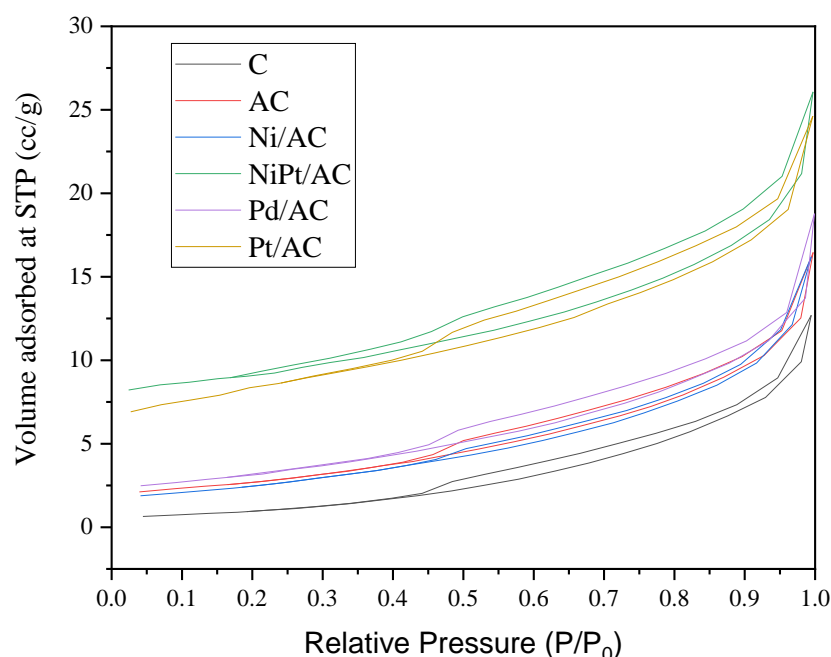


Fig. 5. N₂ adsorption-desorption isotherm of C, AC, Ni/AC, NiPt/AC, Pd/AC, Pt/AC

Table 1. Physical and chemical properties of the catalyst

Catalyst	Specific Surface Area (m ² /g)	Average Pore Diameter (nm)	Total Pore Volume (cm ³ /g)	Micropore Volume (cm ³ /g)	Acidity (mmol/g)
C	3.29	18.46	0.018	0.001	0.84
AC	9.33	9.36	0.023	0.004	1.06
Ni/AC	8.54	10.29	0.024	0.003	1.09
NiPt/AC	31.56	5.03	0.037	0.014	0.98
Pt/AC	29.16	5.21	0.036	0.012	1.13
Pd/AC	10.89	8.20	0.024	0.004	1.10

3.3 Hydrocracking Application

Hydrocracking results using various catalysts are presented in **Table 2**, while the selectivity inside the liquid fraction is disclosed in **Table 3**. Thermal cracking was done as a benchmark for the catalytic activity. Strangely, the AC catalysts give less liquid fraction compared to thermal cracking. This could be explained by the rise of gas fraction when using only AC catalyst, without any metal to guide the reaction selectivity. The metal-supported catalyst has been proven to increase the conversion of the castor oil into liquid fraction. Nevertheless, the substantial abundance of ricinoleic acid presents inherent challenges, given that the primary

objective of hydrocracking is to maximize the yield of hydrocarbons. In this regard, the catalyst's imperative attributes entail proficient hydrodeoxygenation and decarboxylation functionalities.

The liquid fraction exhibits a correlation with the catalyst's acidity, wherein higher acidity tends to yield more liquid fraction, apart from the bimetallic NiPt/AC catalyst. The acidity value plays a pivotal role in the hydrocracking of castor oil into smaller fractions, as it signifies the availability of acid sites for the hydrocracking reaction. Noble metal catalysts, Pt/AC and Pd/AC, demonstrate a similar characteristic in their liquid selectivity, involving the exclusive

decarboxylation of ricinoleic acid. This proposition finds support in the absence of the C13-C18 fraction, which could readily arise from the C12 cleavage of ricinoleic acid. The noble metals predominantly yield alcohol fractions resulting from the the C12 cleavage reaction of ricinoleic acid, while their ability to hydrotreat the alcohol on C12 of ricinoleic acid remains limited. In contrast, Ni/AC employs a distinct hydrocracking pathway for ricinoleic acid, leading to the formation of product fraction in C13-C18 due to hydrodeoxygenation. Although Ni/AC exhibits superior hydrocarbon product formation in the C5-C12 and C13-C18 ranges compared to other monometallic catalysts, the total liquid yield from Ni/AC is comparatively lower than that of the noble metals. This motivates the blending of the two metal catalysts, with Pt chosen for its superior conversion rate.

Synergetic cooperation could be seen in the NiPd/AC catalyst, as the cooperation between the Ni and Pd metals has helped with their metal dispersion across the AC support; the synergetic cooperation also acts in its hydrocracking performance. The bimetallic catalyst showed superiority among the other catalysts, as it has the highest total liquid fraction and hydrocarbon fraction while reducing the formation of gas fraction. The bimetallic catalyst showed totally different hydrocracking product characteristics than the monometallic metal catalyst that, only barely surpassed

the support performance. This surprising performance was owed to the bimetallic system dispersion across AC support. The NiPt/AC catalyst's naturally lower acidity is noteworthy, as it inadvertently prevents the occurrence of over cracking phenomena, which can lead to the formation of undesired gaseous byproducts. These two amazing features that are present in the NiPt/AC catalyst give the catalyst high conversion and good selectivity. This catalyst was chosen for the reusability test.

The reusability test data for the catalyst is presented in **Table 3**. Upon each consecutive use of the catalyst, a notable increase in mass was observed due to the formation of coke on the catalyst surface. This coke deposition appears to impede the catalyst's hydrocracking functionality, leading to a decline in its yield after each cycle and preventing it from achieving the initial performance levels. In comparison to our previous investigation, the NiPt/AC catalyst demonstrates susceptibility to deactivation within just three catalytic cycles and lacks self-regeneration capabilities. This compromised stability can be attributed to its low surface area, which facilitates metal aggregation, as evident from **Fig. 6**. The pronounced metal aggregation emerges as a significant contributing factor to the catalyst deactivation, thereby hindering its overall catalytic activity.

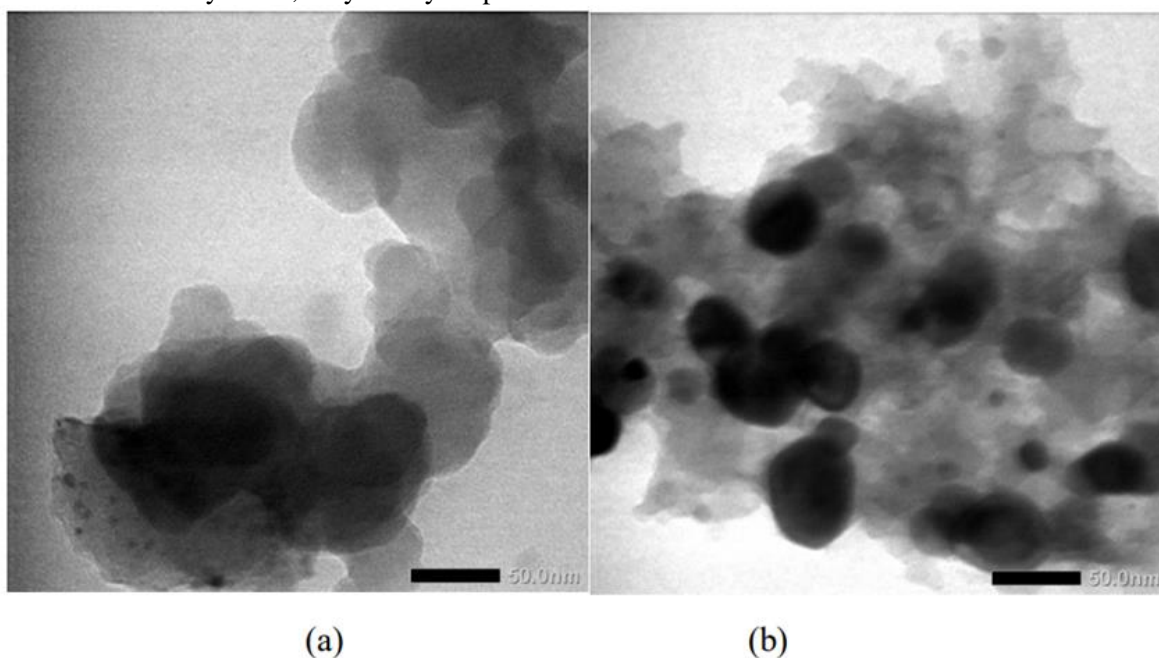


Fig. 6. TEM images of fresh (a) and used (b) NiPd/AC catalyst.

Table 2. Catalyst performance testing on hydrocracking of castor oil

Catalyst	Product Conversion (wt%)			Residue (wt%)
	Liquid	Gas	Coke	
Thermal	84,64	15,06	0,02	0,28
AC	82,22	17,39	0,26	0,13
Ni/AC	84,28	15,39	0,19	0,14
NiPt/AC	88,73	10,17	0,15	0,96
Pt/AC	86,89	12,59	0,43	0,09
Pd/AC	87,94	11,88	0,06	0,13
NiPt/AC #2	88,86	10,36	0,68	0,1
NiPt/AC #3	87,23	11,34	1,13	0,30

Table 3. Catalyst selectivity data towards the liquid fraction

Catalyst	Liquid Fraction (wt%)			Others
	Hydrocarbon		Alcohol	
	C5-C12	C13-C18		
Thermal	5,66	0	59,58	19,25
AC	1,82	0,72	41,59	36,01
Ni/AC	5,84	0,44	73,98	5,92
NiPt/AC	6,66	0	72	10,07
Pt/AC	4,21	0	77,23	5,46
Pd/AC	2,83	0	77,94	7,18
NiPt/AC #2	3,01	0	77,52	8,31
NiPt/AC #3	3,41	0	38,1	48,47

Comparing a catalyst prepared from activated carbon that is prepared using O₂ gas as an activating agent to a pur previous study using the same oil feedstock model [15, 16], the synthesized catalyst has tremendous selectivity to decarboxylating ricinoleic acid, yielding tremendous value of alcoholic compounds. However, the elevated selectivity for decarboxylation introduces a tradeoff, leading to complications such as problematic coke formation, which also leads to reduced catalyst usability.

4. Conclusions

In this research, we found that the optimum temperature to activating the char with O₂ gas is 350°C, as its highest iodine value was fall within this temperature. We also found that monometallic system of Pd and Pt tends to work by decarboxylating the ricinoleic acid rather than cleave the ricinoleic acid at C12. The synergetic effect of bimetallic Ni and Pt metal across AC material gave the catalyst a more specific surface area and porosity,

hence affecting its performance in a positive manner. It was also noted that our catalyst, although it has low porosity properties, they have good job for decarboxylation application that can be explained by the high iodine value of the support material. However, the total system of NiPt/AC did not have good stability as it was deactivated and suffered heavy metal aggregation, and could not give good conversion of ricinoleic acid, marked by its high carboxylic acid compound present in the liquid product.

Acknowledgements

The authors would like to thank Universitas Gadjah Mada for the research facility and instrumentation.

Conflict of Interest

The authors report no declarations of interest.

Author Contribution

Wega Trisunaryanti: Conceptualization, Supervision, Resources, Methodology, Writing - review & editing, funding acquisition. Iip Izul Falah: Methodology, Writing - review & editing. Siti Khoirun Nasifah: Investigation, Methodology, Formal analysis, Visualization. Satriyo Dibyo Sumbogo: Formal Analysis, Visualization, Writing - original draft.

References

- [1] Attaphaiboon, W., Neramittagapong, A., Neramittagapong, S., & Theerakulpisut, S. Potential of vegetable oils for producing green diesel via hydrocracking process. *Thai Environ. Eng. J.*, 35(2), (2021). 1-11.
- [2] El-Sawy, M. S., Hanafi, S. A., Ashour, F., & Aboul-Fotouh, T. M. Co-hydroprocessing and hydrocracking of alternative feed mixture (vacuum gas oil/waste lubricating oil/waste cooking oil) with the aim of producing high quality fuels. *Fuel*, 269, (2020). 117437.
- [3] Mederos-Nieto, F. S., Elizalde-Martínez, I., Trejo-Zárraga, F., Hernández-Altamirano, R., & Alonso-Martínez, F. Dynamic modeling and simulation of three-phase reactors for hydrocracking of vegetable oils. *Reaction Kinetics, Mechanisms and Catalysis*, 131, (2020). 613-644.
- [4] Al Muttaqii, M., Kurniawansyah, F., Prajitno, D. H., & Roesyadi, A. Hydrocracking process of coconut oil using Ni-Zn/HZSM-5 catalyst for hydrocarbon biofuel production. In *Journal of Physics: Conference Series* 1725 (1) (2021) 012008. IOP Publishing.
- [5] Liu, J., Li, Y., He, J., Wang, L., Lei, J., & Rong, L. Ni-based non-sulfided inexpensive catalysts for hydrocracking/Hydrotreating of *Jatropha* oil. *Mini-Rev. Org. Chem.*, 17(2), (2020). 141-147.
- [6] Li, Z., Yang, X., Han, Y., & Rong, L. Hydrocracking of *Jatropha* oil to aromatic compounds over the LaNiMo/ZSM-5 catalyst. *Inter. J. Hydrogen Ener.* 45(41), (2020). 21364-21379.
- [7] Kartika, I. A., Sumbogo, S. D., Fataya, I., Trisunaryanti, W., & Sailah, I. (2022, June). Optimization of *Calophyllum* oil extraction and its application for biogasoline. In *IOP Conference Series: Earth and Environmental Science* (Vol. 1034, No. 1, p. 012035). IOP Publishing.
- [8] Trisunaryanti, W., Sumbogo, S. D., Mukti, R. R., Kartika, I. A., Hartati, & Triyono. Performance of low-content Pd and high-content Co, Ni supported on hierarchical activated carbon for the hydrotreatment of *Calophyllum inophyllum* oil (CIO). *Reaction Kinetics, Mechan. Catal.* 134, (2021). 259-272.
- [9] Trisunaryanti, W., Mukti, R. R., Kartika, I. A., Firda, P. B. D., Sumbogo, S. D., Prasetyoko, D., & Bahruji, H. Highly selective hierarchical ZSM-5 from kaolin for catalytic cracking of *Calophyllum inophyllum* oil to biofuel. *J. Energy Inst.*, 93(6), (2020). 2238-2246.
- [10] Sihombing, J. L., Gea, S., Wirjosentono, B., Agusnar, H., Pulungan, A. N., Herlinawati, H., Yusuf, M., & Hutapea, Y. A. Characteristic and catalytic performance of Co and Co-Mo metal impregnated in sarulla natural zeolite catalyst for hydrocracking of MEFA rubber seed oil into biogasoline fraction. *Catalysts*, 10(1), (2020). 121.
- [11] Singh, S., Sharma, S., Sarma, S. J., & Brar, S. K. A comprehensive review of castor oil-derived renewable and sustainable industrial products. *Environ. Progress Sustain. Energ.*, 42(2), (2023).e14008.
- [12] Chauke, N. P., Mukaya, H. E., & Nkazi, D. B. Chemical modifications of castor oil: A review. *Science Progress*, 102(3), (2019).199-217.
- [13] Yeboah, A., Ying, S., Lu, J., Xie, Y., Amoanimaa-Dede, H., Boateng, K. G. A., Chen, M., & Yin, X. Castor oil (*Ricinus communis*): a review on the chemical composition and physicochemical properties. *Food Sci. Tech.*, 41, (2020). 399-413.
- [14] Meller, E., Gutkin, V., Aizenshtat, Z., & Sasson, Y. Catalytic hydrocracking-hydrogenation of castor oil fatty acid methyl esters over nickel substituted polyoxometalate catalyst. *ChemistrySelect*, 1(20), (2016)6396-6405.
- [15] Trisunaryanti, W., Triyono, T., Purwono, S., Purwanti, A. S., & Sumbogo, S. D. Synthesis of mesoporous carbon from merbau sawdust as a nickel metal catalyst support for castor oil hydrocracking. *Bullet. Chem. Reaction Eng. Catal.*, 17(1), (2022). 216-224.
- [16] Wijaya, K., Syoufian, A., Fitroturokhmah, A., Trisunaryanti, W., Adi Saputra, D., & Hasanudin. Chrom/nanocomposite ZrO₂-pillared bentonite catalyst for castor oil (*ricinus communis*) hydrocracking. *Nano Hybrids and Composites*, 27, (2019)31-37.
- [17] Rorrer, J. E., Ebrahim, A. M., Questell-Santiago, Y., Zhu, J., Troyano-Valls, C., Asundi, A. S., Brenner, A.E., Bare, S.R., Tassone, T.J., Beckham, G.T., & Roman-Leshkov, Y. Role of Bifunctional Ru/Acid Catalysts in the Selective Hydrocracking of Polyethylene and Polypropylene Waste to Liquid Hydrocarbons. *ACS Catal.*, 12(22), (2022). 13969-13979.

- [18] Ma, Y., Liang, R., Wu, W., Zhang, J., Cao, Y., Huang, K., & Jiang, L. Enhancing the activity of MoS₂/SiO₂-Al₂O₃ bifunctional catalysts for suspended-bed hydrocracking of heavy oils by doping with Zr atoms. *Chin. J. Chem. Eng.*, 39, (2021). 126-134.
- [19] Tedstone, A. A., Bin Jumah, A., Asuquo, E., & Garforth, A. A. Transition metal chalcogenide bifunctional catalysts for chemical recycling by plastic hydrocracking: a single-source precursor approach. *Royal Society Open Science*, 9(3), (2022), 211353.
- [20] Trisunaryanti, W., Larasati, S., Bahri, S., lailun Ni'mah, Y., Efiyanti, L., Amri, K., Nuryanto, R., & Sumbogo, S. D. Performance comparison of Ni-Fe loaded on NH₂-functionalized mesoporous silica and beach sand in the hydrotreatment of waste palm cooking oil. *J. Environ. Chem. Eng.*, 8(6), (2020).104477.
- [21] Utami, M., Wijaya, K., & Trisunaryanti, W. Pt-promoted sulfated zirconia as catalyst for hydrocracking of LDPE plastic waste into liquid fuels. *Mater. Chem. Physic.*, 213, (2018)548-555.
- [22] Kusumastuti, H., Trisunaryanti, W., Falah, I. I., & Marsuki, M. F. Synthesis of mesoporous silica-alumina from lapindo mud as a support of Ni and Mo metals catalysts for hydrocracking of pyrolyzed α -cellulose. *Rasayan J Chem*, 11(2), (2018), 522-530.
- [23] Saab, R., Polychronopoulou, K., Anjum, D. H., Charisiou, N., Goula, M. A., Hinder, S. J., Baker, M.A., & Schiffer, A.. Carbon Nanostructure/Zeolite Y Composites as Supports for Monometallic and Bimetallic Hydrocracking Catalysts. *Nanomater.*, 12(18), (2022)3246.
- [24] Jeon, S. G., Na, J. G., Ko, C. H., Yi, K. B., Rho, N. S., & Park, S. B.. Preparation and application of an oil-soluble CoMo bimetallic catalyst for the hydrocracking of oil sands bitumen. *Energy & Fuels*, 25(10), (2011), 4256-4260.
- [25] Kostyniuk, A., Bajec, D., & Likozar, B. Hydrocracking, hydrogenation and isomerization of model biomass tar in a packed bed reactor over bimetallic NiMo zeolite catalysts: Tailoring structure/acidity. *Applied Catalysis A: General*, 612, (2021)118004.
- [26] Trisunaryanti, W., Suarsih, E., & Falah, I. I. Well-dispersed nickel nanoparticles on the external and internal surfaces of SBA-15 for hydrocracking of pyrolyzed α -cellulose. *RSC adv.*, 9(3), (2019). 1230-1237.
- [27] Heidarinejad, Z., Dehghani, M. H., Heidari, M., Javedan, G., Ali, I., & Sillanpää, M. Methods for preparation and activation of activated carbon: a review. *Environ. Chem. Lett.*, 18, (2020) 393-415.
- [28] Yahya, M. A., Al-Qodah, Z., & Ngah, C. Z. Agricultural bio-waste materials as potential sustainable precursors used for activated carbon production: A review. *Renewable and sustainable energy reviews*, 46, (2015) 218-235.
- [29] Santi, D., Trisunaryanti, W., & Falah, I. I. (2022, March). NiO Supported on Porous Carbon From Merbau Wood: Synthesis and Characterization. In *IOP Conference Series: Materials Science and Engineering* (Vol. 1232, No. 1, p. 012001). IOP Publishing.
- [30] Žula, M., Grilc, M., & Likozar, B. Hydrocracking, hydrogenation and hydro-deoxygenation of fatty acids, esters and glycerides: Mechanisms, kinetics and transport phenomena. *Chemical Engineering Journal*, 444, (2022), 136564.
- [31] Marlinda, L., Al-Muttaqii, M., Roesyadi, A., & Prajitno, D. H. (2017, May). Formation of hydrocarbon compounds during the hydrocracking of non-edible vegetable oils with cobalt-nickel supported on hierarchical HZSM-5 catalyst. In *IOP Conference Series: Earth and Environmental Science* (Vol. 67, No. 1, p. 012022). IOP Publishing.
- [32] Al Muttaqii, M., Marlinda, L., Roesyadi, A., & Prajitno, D. H. Co-Ni/HZSM-5 catalyst for hydrocracking of Sunan candlenut oil (*Reutealis trisperma* (Blanco) airy shaw) for production of biofuel. *J. Pure Applied Chem. Res.*, 6(2), (2017) 84.
- [33] Cheng, J., Zhang, Z., Zhang, X., Liu, J., Zhou, J., Cen, K. Hydrodeoxygenation and hydrocracking of microalgae biodiesel to produce jet biofuel over H3PW12O40-Ni/hierarchical mesoporous zeolite Y catalyst. *Fuel*, 245, (2019) 384-391.
- [34] Yi, H., Nakabayashi, K., Yoon, S. H., & Miyawaki, J. Pressurized physical activation: A simple production method for activated carbon with a highly developed pore structure. *Carbon*, 183, (2021) 735-742.
- [35] Ding, Y., Qi, J., Hou, R., Liu, B., Yao, S., Lang, J. & Yang, B. Preparation of high-performance hierarchical porous activated carbon via a multistep physical activation method for supercapacitors. *Energy & Fuels*, 36(10), (2022) 5456-5464.
- [36] Gao, Y., Yue, Q., Gao, B., & Li, A.. Insight into activated carbon from different kinds of chemical activating agents: A review. *Sci. Total Env.*, 746, (2020)141094.

[37] Gayathiri, M., Pulingam, T., Lee, K. T., & Sudesh, K. Activated carbon from biomass waste precursors: Factors affecting production and adsorption mechanism. *Chemosphere*, 294, (2022). 133764.

[38] Mariana, M., HPS, A. K., Mistar, E. M., Yahya, E. B., Alfatah, T., Danish, M., & Amayreh, M.. Recent advances in activated carbon modification techniques for enhanced heavy metal adsorption. *J. Water Process Eng.*, 43, (2021) 102221.

[39] Saleem, J., Shahid, U. B., Hijab, M., Mackey, H., & McKay, G.. Production and applications of activated carbons as adsorbents from olive stones. *Biomass Conver. Bioref.*, 9, (2019) 775-802.

[40] Mopoung, S., Moonsri, P., Palas, W., & Khumpai, S. (2015). Characterization and properties of activated carbon prepared from tamarind seeds by KOH activation for Fe (III) adsorption from aqueous solution. *The scientific world journal*, 2015.